Polymer Alloys Based on Poly(2,6-dimethyl-1,4-phenylene ether) and Poly(styrene-*co*-acrylonitrile) Using Poly(styrene-*b*-(ethylene-*co*-butylene)-*b*-methyl methacrylate) Triblock Copolymers as Compatibilizers

Clemens Auschra and Reimund Stadler*

Institut für Organische Chemie, Johannes Gutenberg Universität Mainz, J. J. Becherweg 18-20, D-6500 Mainz, Germany

Received May 5, 1993; Revised Manuscript Received August 27, 1993®

ABSTRACT: Poly(styrene-*b*-(ethylene-*co*-butylene)-*b*-methyl methacrylate) (P(S-*b*-EB-*b*-MMA) triblock copolymers containing various amounts of the elastomeric center block (6–38 wt % PEB) have been used to compatibilize polymer blends based on poly(2,6-dimethyl-1,4-phenylene ether) (PPE) and poly(styrene-*co*-acrylonitrile) (PSAN). From the dynamic mechanical analysis in combination with transmission electron microscopy detailed information about the location of the block copolymers is obtained, because the intermixing of the PS block with PPE and the PMMA block with PSAN changes the glass transitions of the main components. In all studied blends, the PS block penetrates into the PPE. In blends with PSAN20, a copolymer containing 20 wt % acrylonitrile, the PMMA block is mixed with PSAN, while this is not the case in blends with PSAN43 (43 wt % acrylonitrile). In blends with PSAN20 the elastomeric center block (PEB) does not form a rubbery layer along the PPE/PSAN interface. Due to the large incompatibility between PEB and all other blend components small rubber islands form at the PPE/PSAN boundary, giving rise to a "raspberry" type morphology. The location of these rubbery particles at the interface causes a considerable improvement of the mechanical interfacial strength. Stable bicontinuous morphologies are formed at PSAN:PPE ratios around 60:40.

Introduction

Block copolymers have found widespread interest as compatibilizing agents for immiscible polymer blends.[1] However, the use of poly(A-*b*-B) block copolymers as compatibilizers of poly(A)/poly(B) blends often does not result in an improvement of the mechanical phase adhesion, though the block copolymer is an efficient dispersing agent. The major reasons discussed in the literature for this observed deficiency is the formation of a "dry brush" situation at too low molecular weights[2] and the balance between compatibilizing efficiency and micelle formation.[3,4] Figure 1 gives a schematic representation of these different situations of a block copolymer in an A/B blend. An efficient mechanical coupling will only be achieved if each block of the block copolymer intimately mixes with one of the blend components (wet brush). If the segments of the block copolymer and the blend components do not interpenetrate (dry brush), this may cause a weak mechanical link despite the fact that the block copolymer reduces the surface tension. There has been some discussion how the dry brush/wet brush balance is influenced by the ratio of block length and molecular weights of the blend components.[2,3] While large block copolymers should act as more efficient compatibilizers, they also tend to form micelles at concentrations larger than the corresponding critical micelle concentration (Figure 1c).[3-6] Both problems discussed should be avoidable, if a block copolymer poly(C-*b*-D) is used as a compatibilizer for poly(A)/poly(B) blends, in which each block of the block copolymer is chemically different but thermodynamically miscible with one of the blend components. The negative enthalpic interaction between A/C and B/D enforces interpenetration and thus the wet brush situation. Additionally, the location of the CD block copolymer at the A/B interface is thermodynamically favored in comparison to the formation of block copolymer micelles in either of the two phases. This situation has recently been treated theoretically by Braun et al.[7]

In previous work[8,9] we have shown that such a system is realized in blends of PPE and PSAN20 using P(S-*b*-MMA) diblock copolymers of variable molecular weight as compatibilizer. In this system the PS block has a thermodynamic driving force to enter the PPE domain ($\chi_{S/PE} = -0.1$)[10] while the PMMA block is miscible with PSAN copolymers, if the acrylonitrile (AN) content is 20 wt % ($\chi_{PSAN20/PMMA} \approx -0.008$).[11] If the acrylonitrile content is larger than about 35 wt % the interaction turns positive ($\chi_{PSAN43/PMMA} \approx +0.005$).[8,11] As a result the block copolymer locates at the interphase in the case of PSAN20/PPE blends and penetrates into the blend components.[8,9] Nevertheless the mechanical strength of the blends as measured by stress–strain experiments on bulk samples remained unsatisfactory (see below).[14] Recent experiments by Brown et al.[5] on PPE/P(S-*b*-MMA)/PMMA and PS/P(S-*b*-MMA)/PMMA layers demonstrate an increased strength of the single layer.

Thus another argument to explain the low ultimate mechanical properties in blends of a rubber toughened PSAN (matrix) with dispersed PPE and added P(S-*b*-MMA) diblock has been proposed: Both PPE and PSAN are amorphous polymers under the present conditions. Upon cooling a blend (with or without compatibilizer) from the melt, the high T_g component (PPE) freezes first. In the temperature range between the glass transitions of the two major components the respective thermal expansion coefficients are quite different. This may cause mechanical stresses at the phase boundary, which could give rise to the low ultimate mechanical properties of the blend. The results reported in the literature that tapered block copolymer systems are more efficient in terms of mechanical compatibilization[15,16] can also be rationalized along the same argument.

Based on this consideration it is straightforward to use a compatibilizer which could avoid the formation of

* To whom all correspondence should be addressed.
® Abstract published in *Advance ACS Abstracts*, October 15, 1993.

0024-9297/93/2226-6364$04.00/0

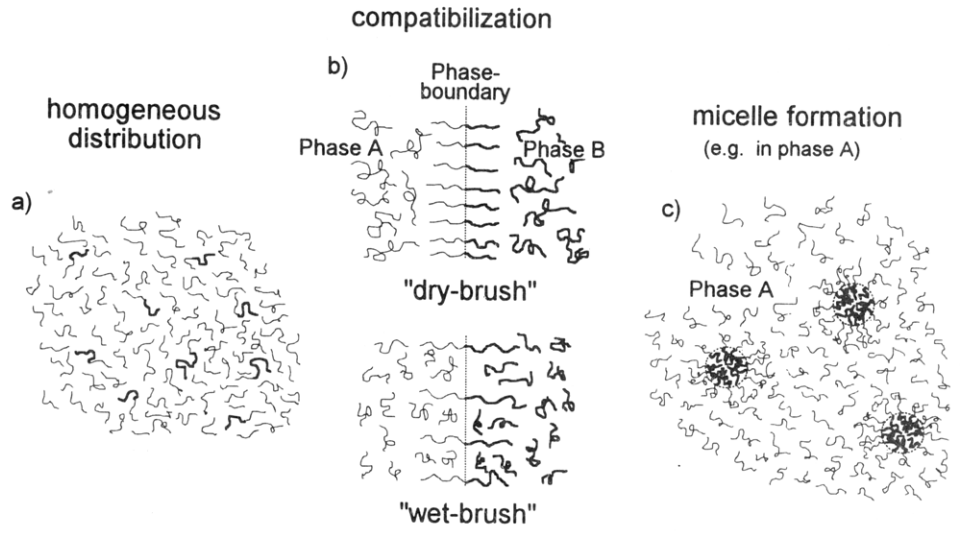

Figure 1. A-*b*-B block copolymers as additives to a binary A/B polymer: (a) homogeneous distribution of the block copolymer in both components; (b) localization of the block copolymer at the A/B interface [(b-1) dry brush, (b-2) wet brush]; (c) block copolymer micelles in one or both blend conponents.

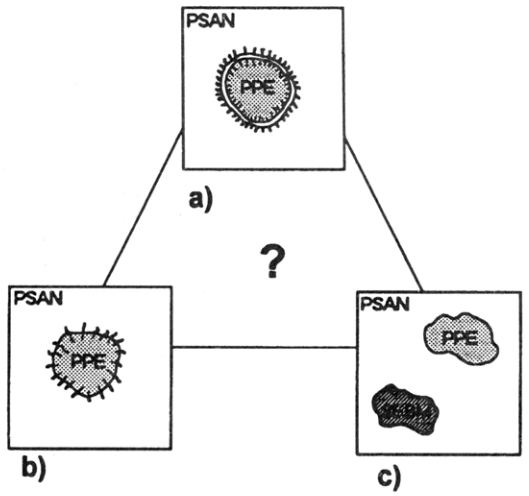

Figure 2. Possible morphologies of blends of PPE and PSAN containing P(S-*b*-EB-*b*-MMA) triblock copolymers: (a) block copolymer with elastomer block of intermediate length; (b) very short elastomer block (same behavior as P(S-*b*-MMA) diblock); (c) large elastomer block (large elastomer volume fraction) (macrophase separation).

internal stresses at the interface. For this purpose we have synthesized poly(styrene-*b*-(ethylene-*co*-butylene)-*b*-methyl methacrylate) (P(S-*b*-EB-*b*-MMA)) block copolymers via sequential anionic polymerization of stryrene, butadiene, and methyl methacrylate and subsequent hydrogenation of the butadiene block.[17] If this block copolymer would locate at the interface of a PPE/PSAN20 blend, a thin elastomeric layer between the glassy blend components could form, resulting in an efficient reduction of the mechanical stresses below the glass transitions of PPE and PSAN. Figure 2 shows the extreme situations of blend morphologies that could be expected upon variation of the center block length. While a very long center block could result in a macroscopic phase separation (Figure 2c), a very short center block would represent the crossover to the diblock situation (Figure 2b). Thus it might be expected that a block copolymer of intermediate length would be most suited. In addition the tendency toward micelle formation might be influenced by the center block. However, as will be discussed below, the actual morphology formed at the phase boundary in the present system differs considerably from the schematic picture given in Figure 2a.

As we have shown recently, the morphology of ABC triblock copolymers is governed not only by the volume fractions ϕ_A, ϕ_B, and ϕ_C but also by the balance of the three binary interaction parameters $\chi_{A/B}$, $\chi_{B/C}$, and $\chi_{A/C}$ which also are related to the corresponding interfacial energies.[14,18] In most reported triblock copolymer systems like in P(S-*b*-I-*b*-MMA)[19] or P(S-*b*-I-*b*-VP)[20-24] the incompatibility of the two end blocks is larger than the incompatibility of one of the end blocks with the center block ($\chi_{13} > \chi_{12}$ or χ_{23}). As a consequence the sequence of phase boundaries follows the block sequence, i.e. there are no A/C boundaries. In the case of P(S-*b*-EB-*b*-MMA) block copolymers the hydrogenated butadiene block dislikes the two end blocks more than these dislike each other: $\chi_{PS/PEB} \sim \chi_{PMMA/EB} \gg \chi_{PS,PMMA}$. As a consequence the system will tend to minimize the phase boundary PS/PEB and PMMA/PEB at the expense of creating PS/PMMA boundaries. New regular morphologies result from this thermodynamic balance.[14,18] As will be discussed below, the same thermodynamic arguments can be applied to the blends discussed here. To elucidate the influence of added SEBM triblock copolymers in detail, the present paper deals with dynamic mechanical and morphological studies in the following systems (Figure 3). In section A the main emphasis addresses the question whether the P(S-*b*-EB-*b*-MMA) block copolymers actually locate at the interface and which morphologies result. As in the previous study[8,9] where P(S-*b*-MMA) diblock copolymers have been used as compatibilizers, ternary blends with PPE and either PSAN20 (which is miscible with PMMA) or PSAN43 (which is immiscible with PMMA) will be compared for this purpose.

In section B the PSAN20/PPE composition will be varied at relatively large amounts of block copolymer. In section C the influence of the length of the elastomeric center block of the block copolymer is studied with the limit of the P(S-*b*-MMA) diblock. Special emphasis is given to blends with a dispersed PPE phase. Preliminary experiments on the fracture behavior of the blends compatibilized with the triblock copolymer will be reported in section D.

Experimental Section

Materials. P(S-*b*-EB-*b*-MMA) triblock copolymers were obtained by sequential anionic polymerization. The experimental details developed to avoid termination during the polymerization

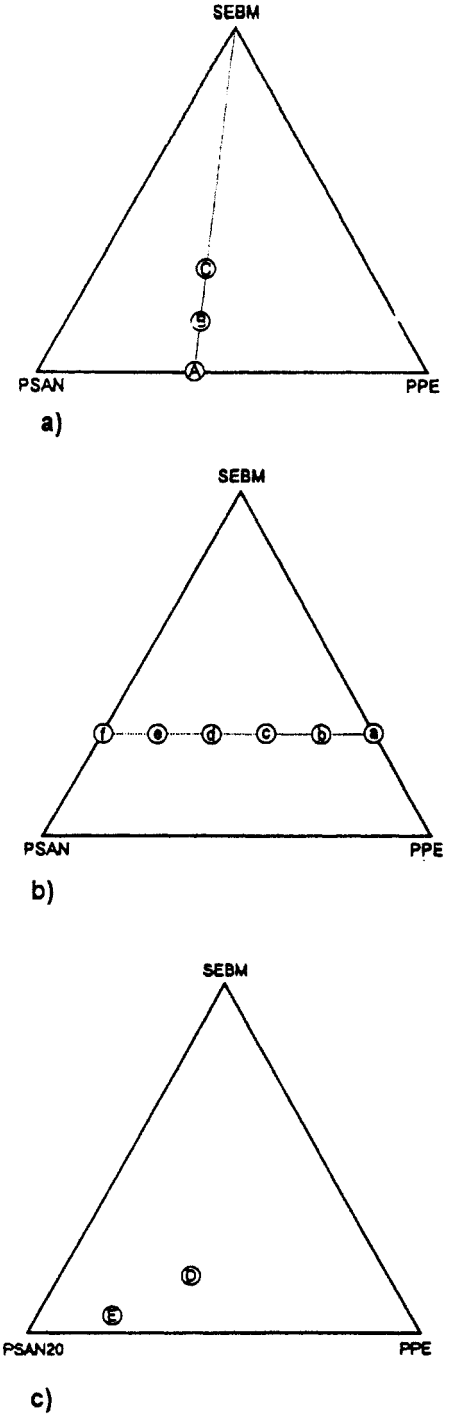

Figure 3. Illustration of the blend compositions used in this study: (a) compositions PSAN/PPE 60:40 without (A) and with 15 (B, B') and 30 (C, C') wt % added triblock copolymer SEBM38 [variation of styrene acrylonitrile copolymer (PSAN20 and PSAN43)]; (b) variation of PSAN20/PPE composition (a–f). (c) Variation of the triblock copolymers SEBM38, SEBM17, and SEBM6 at two compositions (D, E).

of the butadiene block in THF are reported elsewhere.[17] The P(EB-*b*-MMA) diblock copolymer used to toughen PSAN20 (see section D) and the P(S-*b*-MMA) diblock copolymer SM97, were obtained in a similar way. All block copolymers have a narrow molecular weight distribution with no detectable homopolymer impurities. The polybutadiene block was hydrogenated by the reaction with diimine[25] using *p*-toluenesulfonic hydrazide as the diimine source. The thermal stability of the block copolymers has been studied separately.[26] The detailed analytical results obtained for the P(S-*b*-EB-*b*-MMA) and P(EB-*b*-MMA) block copolymers are given in Table I. Number average molecular weights were determined osmometrically,[27] and the polydispersity and block copolymer purity, by GPC. Hydrogenation resulted only in a negligible increase of the polydispersity.[17] The PSAN20

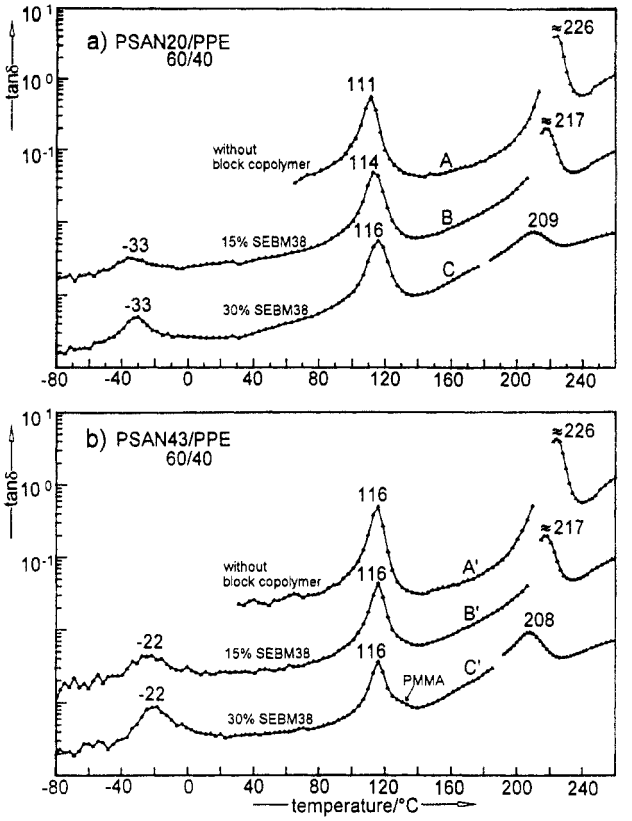

Figure 4. Dynamic mechanical analysis of ternary blends PSAN/PPE/SEBM38: (a) PSAN20; (b) PSAN43. Compositions are according to Table III. For data at temperatures up to about 140–170 °C, dual cantilever (DC) geometry; At higher temperatures, shear sandwich (SSW) geometry. The curves are shifted vertically for one decade. The ordinate scale is valid for the upper curve.

and PSAN43 copolymers were kindly provided by BASF AG (Ludwigshafen). The materials were fractionated to remove low molecular weight components. Poly(2,6-dimethyl-1,4-phenylene ether) (PPE) was prepared from 2,6-dimethyl-4-bromophenol according to the method described by Percec et al.[28] The PPE was endcapped to avoid the equilibration reaction and fractionated to remove low molar mass material. Details of the experimental procedures are given in ref 8.

Table II summarizes the analytical data of the blend components and gives the glass transitions obtained by DSC (10 K min^{-1}) and dynamic mechanical analysis at 1 rad s^{-1}.

The thermal stability of all components was checked carefully. The most sensitive component is the PMMA block. Substantial depolymerization of the PMMA block occurs at temperatures above 245 °C.[26]

Conditions for blend preparations were the same as in our previous work:[8] The blends were prepared by coprecipitation of the mixture of the components from dilute solution (1.2–1.5% w/v in THF). The fine powders obtained by this procedure were carefully dried under vacuum (50–80 °C) for several days and then put into a melt press which allows the preparation of the samples under vacuum. The samples were kept at 240 °C for 45 min. By this technique bubble-free specimens were obtained. In our previous study we have demonstrated that this annealing is sufficient to approach the equilibrium structure without complications related to significant degradation.[8]

Methods. Dynamic mechanical measurements were performed on a Rheometrics Solids Analyzer RSAII in the temperature step mode at a constant frequency of 1 rad s^{-1} and a delay time of 1 min before each measurement. Strains were kept small enough to ensure linear viscoelastic behavior. To cover the mechanical behavior in a wide range, the blends were tested with two different test geometries: *dual cantilever* (DC) (45 mm × 6 mm × 2.3 mm) for the modulus range with $E' > 10^8$ Pa and *shear sandwich* (SSW) (2 × (2 mm × 5.5 mm × 55 mm)) in the region with $G' < 10^7$ Pa. In the SSW geometry samples were

Table I. Analytical Results of the Block Copolymers[a]

	PS		P(S-*b*-B)		P(S-*b*-B-*b*-MMA)			
BC	M_n	M_w/M_n	M_n	M_w/M_n	M_n	M_w/M_n	w_{PS}	w_{PB}
SBM6	80 (GPC) 88 (osmosis)	1.04	(93) 96	1.06	(165) 225	1.11	0.45	0.06
SBM17	100 (GPC) 108 (osmosis)	1.05	(148) 145	1.06	(205) 238	1.10	0.48	0.17
SBM38	57 (GPC) 64 (osmosis)	1.04	(135) 175	1.07	(189) 245	1.08	0.24	0.38

	PB		P(B-*b*-MMA)		
	M_n	M_w/M_n	M_n	M_w/M_n	w_{PB}
BM63	(55) (GPC)	1.09	(84)	1.10	0.63

	PS		P(S-*b*-MMA)		
	M_n	M_w/M_n	M_n	M_w/M_n	w_{PS}
SM97	97 (GPC) 92 (osmosis)	1.12	(180) 205	1.13	0.47

[a] Analytical results of the unhydrogenated block copolymers and their PS and P(S-*b*-B) precursors which were isolated during anionic polymerization. SBM = poly(styrene-*b*-butadiene-*b*-methyl methacrylate); BM = poly(butadiene-*b*-methyl methacrylate). In the text the corresponding hydrogenated block copolymers are denoted as SEBM and EBM. The polybutadiene block of the copolymers consists predominantly of 1,2-vinylic structures (≈90 mol % 1,2-units). GPC: THF; in brackets, molecular weights of the block copolymers and precursors appear somewhat too low due to PS calibration. w_{PS}, w_{PB} = weight fraction of PS and PB determined from ^{1}H NMR.

Table II. Characteristics of Blend Components

				T_g/°C		
polymer	M_n	M_w/M_n	w_s	DSC[e]	E''_{max}[f]	tan δ_{max}[f]
PSAN20	(166)[a] 160[c]	1.60	0.89[d]	110	110	113
PSAN43	(45)[a]	1.40	0.57[d]	111	114	116
PPE-II	(105)[b] 90[c]	2.0		215	216	227

[a] GPC in THF. [b] GPC in $CHCl_3$; PS calibration. [c] Membrane osmosis in $CHCl_3$. [d] Weight fraction of styrene determined from elemental analysis. [e] DSC: heating rate = 10 K/min. [f] Temperature of the maximum of the E'' and tan δ peaks at a frequency of 1 rad/s.

Table III[a]

(a) Blends with PSAN20

blend	w_{PMMA}	w_{PS}	PSAN20	PPE-II	SEBM38
A	0	0	60	40	0
B	0.101	0.096	51	34	15
C	0.263	0.205	42	28	30

(b) Blends with PSAN43

blend	w_{PMMA}	w_{PS}	PSAN43	PPE-II	SEBM38
A′	0	0	60	40	0
B′	0.101	0.096	51	34	15
C′	0.263	0.205	42	28	30

[a] w_{PMMA} = weight fraction of PMMA on the basis of PMMA and PSAN; w_{PS} = weight fraction PS on the basis PS and PPE.

annealed in the instrument at 240 °C to allow good mechanical contact between the plates and the sample.

Stress–strain experiments and fracture tests were make on a home-built stress–strain apparatus. Dumbbell-shaped samples with an efficient zone of 25 mm × 5 mm × 1 mm were used. The strain rate was 1 mm/min^{-1} at an initial sample length of 25 mm.

Transmission Electron Microscopy. Ultrathin sections (50 nm) were cut at room temperature from the specimen used for mechanical testing with a Reichert Ultramicrotome FC4 equipped with a diamond knife. Contrasting was performed by exposing the ultrathin sections on gold grids to RuO_4 vapor according to the method of Trent et al.[29] By variation of the exposure time (10–30 min) at 32–35 °C, different contrasts between the phases could be achieved (see below). Bright field images were taken at an acceleration voltage of 80 kV.

Results and Discussion

A. PSAN43 and PSAN20 in Ternary Blends with PPE and P(S-*b*-EB-*b*-MMA). According to the original idea P(S-*b*-EB-*b*-MMA) triblock copolymers could locate at the phase boundary in PPE/PSAN20 blends and cover the PPE domains with a thin elastomeric layer. To check whether this actually happens, blends with both PSAN20 and PSAN43 are studied. Because the PMMA block is miscible with PSAN20, while it is immiscible with PSAN43, a different behavior can be expected for the two copolymers.[8] Blends with relatively large amounts of SEBM38 were studied. This allows the analysis of the glass transition of all components.

Figure 3a and Table IIIa,b summarize the blend compositions used for this purpose. All blends containing PSAN43 were opaque while blends containing PSAN20 were only slightly turbid (not as transparent as corre-

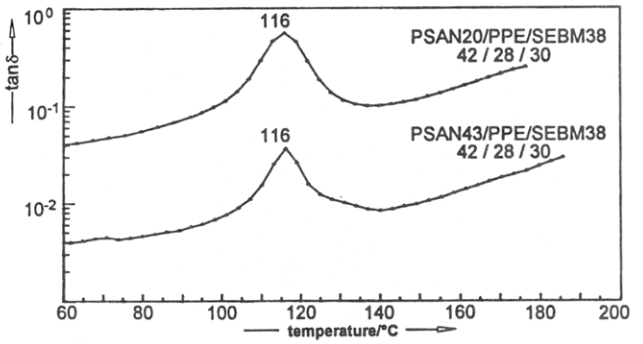

Figure 5. Direct comparison of the loss tangent (tan δ) in the range of the PSAN glass transition $T_{g(PSAN)}$ in blends containing 30 wt % SEBM38. The lower curve is shifted by one decade.

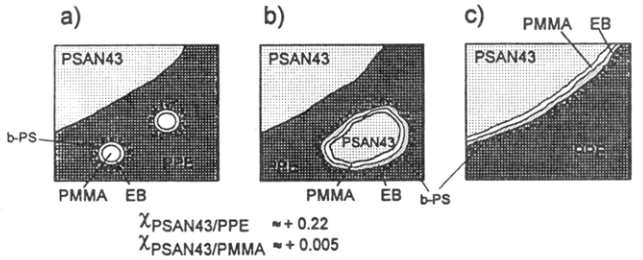

Figure 6. Morphological arrangements of the SEBM38 triblock copolymer in PPE/PSAN43 blends: (a) PMMA cores surrounded by a PEB layer with a PS shell which is mixed with the PPE; (b) and (c) PMMA→PEB→PS layer surrounding small PSAN43 inclusions or large PSAN43 particles.

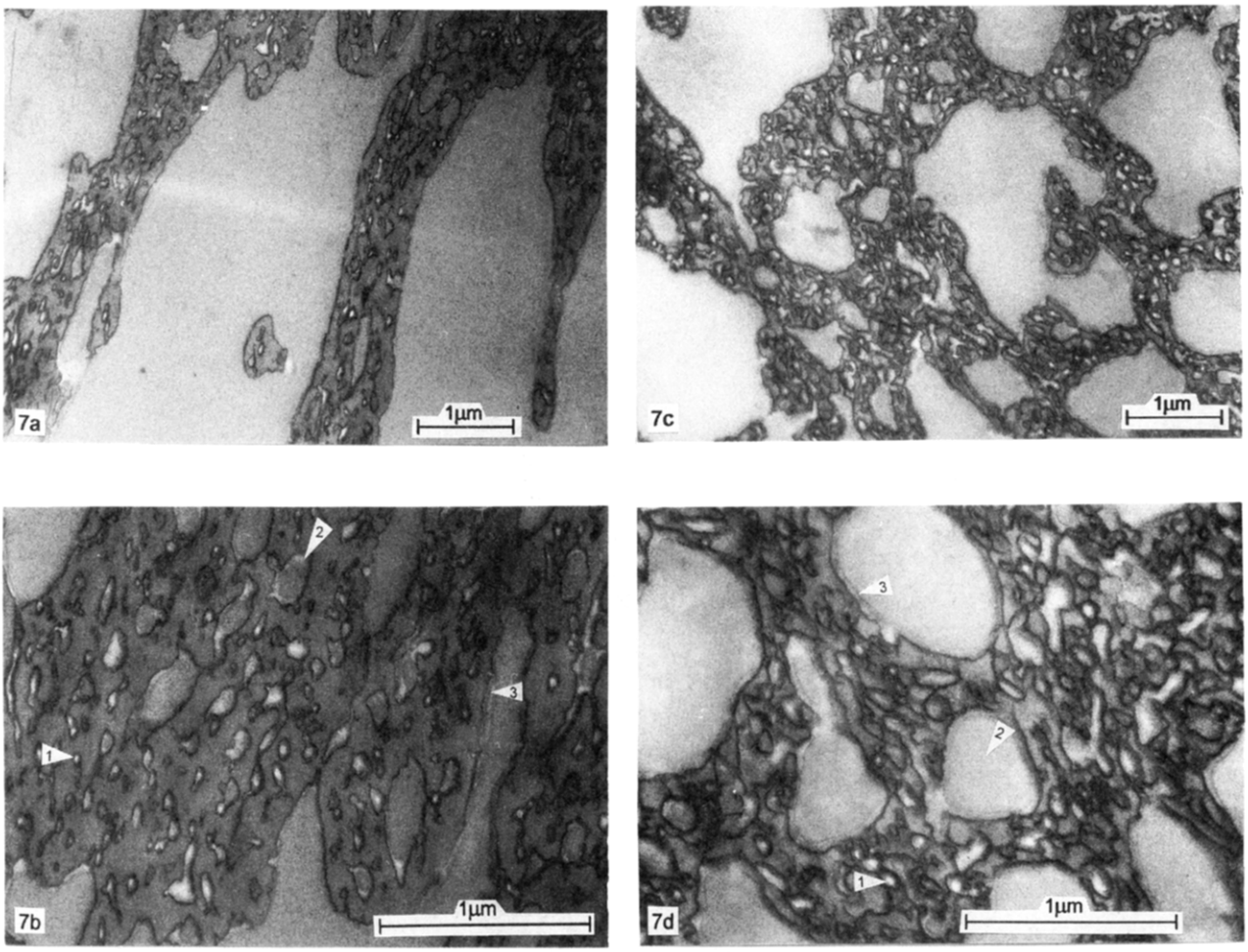

Figure 7. TEM micrographs of ternary PSAN43/PPE/SEBM38 blends (ultrathin sections stained with RuO_4: (dark) PPE; (bright) PSAN): (a) overview image of blend composition B′ (51:34:15); (b) detailed image (larger magnification) of composition B′ (51:34:15); (c) overview image of blend composition C′ (42:28:30); (d) detailed image (larger magnification) of composition C′ (42:28:30). Key: **1** = core shell micelles; **2** = core shell inclusions; **3** separate block copolymer layer at the PSAN43/PPE phase boundary (without penetration of the block copolymer into the phases).

sponding blends containing P(S-*b*-MMA) diblocks). Due to the similar refractive indices of PSAN20 and PPE this only means that the triblock copolymer is not macrophase separated in the ternary blend. Figure 4a,b shows the results of the dynamic mechanical analysis for the two series. In blends with PSAN20 addition of the triblock copolymer slightly increases the PSAN20 glass transition. The weight fraction of PMMA, $w_{PMMA} = m_{PMMA}/(m_{PMMA} + m_{PSAN})$, is 0, 0.1, and 0.26. For a homogeneously mixed PSAN20/PMMA phase the expected increase of the glass transition ΔT_g at $w_{PMMA} = 0.26$ is on the order of 4 K,[9] which is in good agreement with the observed value ($\Delta T_g \approx 5$ K), indicating a rather homogeneous mixing of PSAN20 with the PMMA block.

The lowering and the shape of the PPE glass transition has been used as a sensitive measure of the segment distribution of the PS block in the PPE phase.[9] As can be seen in Figure 4 the PPE glass transition shifts to lower temperatures. Homogeneous binary blends of PS and PPE of the same composition ($w_{PPE} = m_{PPE}/(m_{PS} + m_{PPE})$) would have glass transitions of 213 and 198 °C.[9,30,31] The respective values of the blends are 217 and 209 °C with a broad should toward lower temperatures. This indicates a considerable but not completely homogeneous mixing of the PS block with PPE. The PS block has a molecular weight of 57k. The behavior of a P(S-*b*-MMA) diblock of comparable PS molecular weight is very similar.[9] Both the analysis of the PPE and the PSAN20 glass transition show that the block copolymer is only located at the PPE/PSAN20 interface as in the case of added diblock.

Characteristic differences are observed in blends containing PSAN43 (Figure 4b). While the glass transition related to the mixed PPE/PS phase shows the same concentration dependence, the glass transition of PSAN43 does not change upon addition of the block copolymer. Moreover, a shoulder at high temperatures indicates a separate glass transition of the PMMA block in the blend containing 30 wt % of SEBM38. Figure 5 shows the enlarged section of the (tan δ)/T curve at the PSAN glass transition for the two blends containing 30 wt % SEBM38 to illustrate explicitly the differences between the two different PSAN copolymers. Similar observations have been made with added diblock copolymer.[8] The glass transition of the PMMA block in the pure triblock copolymer (high fraction of syndiotactic diads) according to DMA is 130 °C (E''_{max}; 134 °C at tan δ_{max}).

Another important observation relates to the glass transition of the PEB block. In blends with PSAN43 the PEB glass transition (tan δ_{max}) is located around −22 °C, a value which is the same as in the pure triblock (−24 °C)[14,32] or the P(EB-*b*-MMA) diblock with a PEB matrix (−22 °C).[14] In contrast the PEB glass transition is shifted to −33 °C in the blends with PSAN20. As is discussed elsewhere,[32] this lower T_g as compared to that of the bulk elastomer is indicative for isolated confined PEB microdomains, whose flexible chains are linked to the glassy matrix. The fact that this is not observed in the blends with PSAN43 indicates that the PEB domains are not

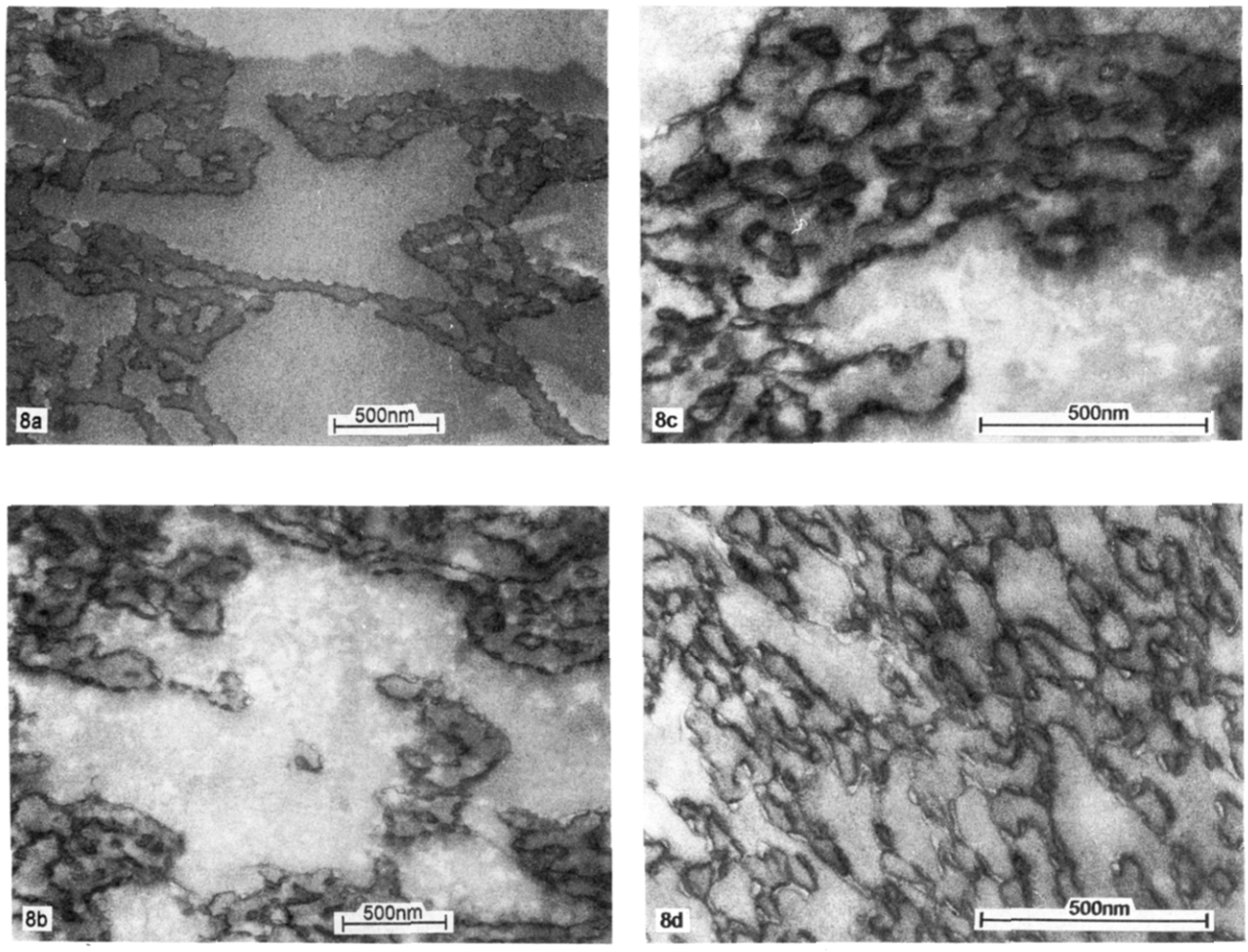

Figure 8. TEM micrograph of ternary PSAN20/PPE/SEBM38 blends (ultrathin sections stained with RuO_4). (a) Blend composition 50:34:16 (staining technique B; see Figure 9b): (bright) PSAN20; (dark) PPE. PEB microdomains are detectable as regular indents along the PPE/PSAN20 phase boundary. (b) and (c) Blend composition 51:35:15 (staining technique A, see Figure 9a): enhanced contrast at the phase boundary, lower (b) and higher (c) magnification. (d) Blend composition C 42:28:30 (staining technique A): enhanced contrast at the phase boundary.

isolated particles with good phase adhesion to the glassy matrix. A similar lowering of the glass transition in blends of diblocks with one identical homopolymer has been observed by Bates and Cohen.[33] They attributed the effect to the effect of interfacial tension.

From the dynamic mechanical data we thus expect the following characteristic features for the morphology of PSAN43/PPE blends with SEBM38 (Figure 6): SEBM38 should be present as lamellae or extended layers. In analogy to the behavior of P(S-*b*-MMA) diblock copolymers where micelles with a PMMA core and a shell of mixed *b*-PS/PPE were dispersed in the PPE, the triblock could be arranged in the PSAN43/PPE/SEBM38 blend (Figure 6a). In addition the block copolymer could form a layer at the PSAN43/PPE boundary. This follows from the larger incompatibility between PSAN43 and PPE as compared to that between PSAN43 and PMMA ($\chi_{PSAN43/PPE} \approx 0.22$; $\chi_{PSAN43/PMMA} \approx 0.005$). As a consequence a layer made out of the PMMA and the PEB block could surround the PSAN43 domain. The PEB phase thus forms as extended layer (which explains the higher T_g) to avoid a high energy PPE/PMMA interface ($\chi_{PPE/PMMA} = +0.5$). The PS blocks are mixed with PPE.

These considerations based on the dynamic mechanical data and thermodynamic arguments are supported by TEM. Figure 7a–d shows the morphology of these PPE/PSAN43/SEBM38 blends. Due to the staining conditions PPE is dark and PSAN43 light. The contrast along the phase boundaries is enhanced.[34] The lower magnifications (Figure 7a,c) show large pure PSAN particles with sizes of several microns. Increasing the amount of SEBM38 slightly reduces the size of the PSAN43 particles. The PPE phase shows the presence of a large amount of PSAN43 inclusions in the submicron size. At the higher magnifications all structural details proposed from the DMA analysis are observable. Besides core shell micelles [1], the PSAN43 inclusions both in the PPE phase [2] and at the phase boundary between the PPE and the large PSAN43 particles show a layered structure with a continuous PEB layer along the phase boundary [3]. The system avoids any PPE/PSAN43 phase boundary. This morphology considerably differs from corresponding blends with P(S-*b*-MMA) diblock copolymers, where no enrichment of the block copolymer close to the PPE/PSAN43 phase boundary was observed.[8] The presence of the elastomeric center block influences the blend morphology. The structure of the PPE phase explains the considerable lowering of the PPE glass transition in the presence of the block copolymer. Starting from the phase boundary, the PS chains can penetrate nearly homogeneously into the PPE phase.

In blends with PSAN20 a completely different morphology is realized. As already deduced from the dynamic mechanical data (shift of $T_{g(PEB)}$, isolated PEB microdomains are expected.[32] Parts a–d of Figure 8 show the morphology of blends containing different amounts of SEBM38 at the same PSAN20:PPE ratio (60:40). Parts a and b of Figure 8 show different magnifications of

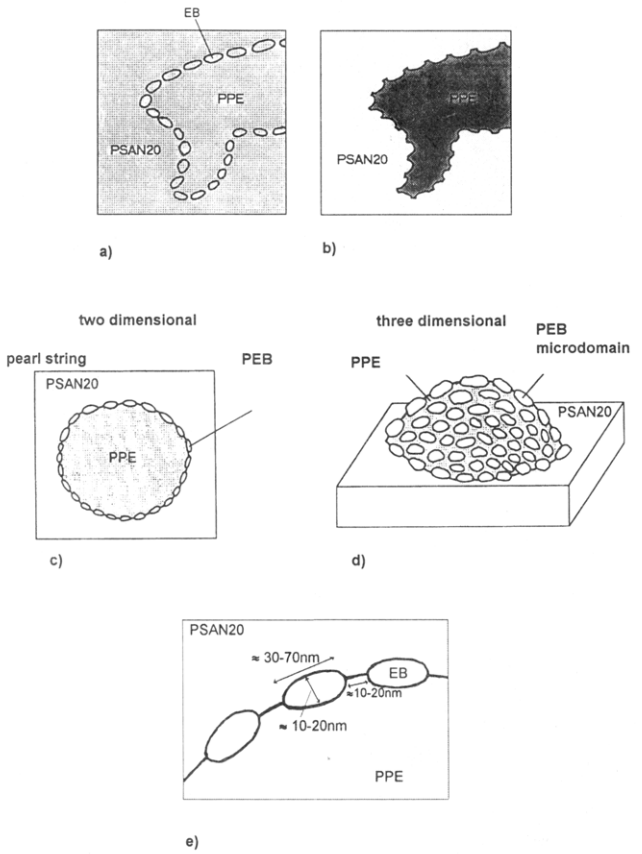

Figure 9. Schematic representation of the morphology of PSAN20/PPE/SEBM38 alloys with a large amount of block copolymer, as visualized by TEM: (a) (staining technique A) enhanced contrast of the PEB phase boundary, no contrast between PPE and PSAN20; (b) (staining technique B) strong contrast between PSAN20 and PPE, no contrast between PSAN20 and PEB and no enhanced contrast at the PSAN20/PEB phase boundary; (c) two-dimensional pearl string morphology of the PEB microdomains along the PSAN20/PPE interface; (d) three-dimensional reconstruction of the morphology of PSAN20/PPE/SEBM38 blends (raspberry morphology); (e) analysis of the PEB microdomain dimensions.

ultrathin sections, where the PPE is stained to a larger extent than PSAN and the phase boundary shows no enhanced contrast. A distinction between PEB and PSAN20 cannot be made. The boundary of the PPE particles has a very peculiar structure with regular indents. These regular indents which have dimensions on the order of 60 nm are the result of the formation of isolated PEB microdomains located at the PPE/PSAN phase boundary. Using the same staining conditions as for the micrographs shown in Figure 7, no contrast between PPE and PSAN20 is formed (Figure 8c,d). However, the phase boundary is stained, and the PEB domains are detectable as a pearl string along the PPE/PSAN20 phase boundary. A similar enhanced contrast formation at the boundary was observed in the pure block copolymers:[18] While in the lamellar SEBM38 the PEB/PMMA boundary was not stained, the phase boundary in SEBM17, where cylinders of PEB are formed at the PS/PMMA interface, was clearly detected.

Figure 9 gives a schematic representation of the morphology in these PPE/SEBM/PSAN20 blends. In Figure 9a,b the different staining conditions which give rise to the different pictures are shown schematically. The presence of isolated PEB microdomains can be recognized by the regular indents (Figure 8a,b). Without complementary pictures like Figure 8c,d and the dynamic mechanical analysis it would be impossible to reconstruct the morphology. However, staining method B (Figure 9b) has the advantage that the PPE/PSAN phase boundary shows up with sharp contrast, thus allowing the detection of the PEB domains as regular indents. In the case of staining method A the phase boundary often appears rather diffuse. Thus the detection of smaller PEB microdomains as they could be expected in blends with SEBM17 and SEBM6 would be impossible.

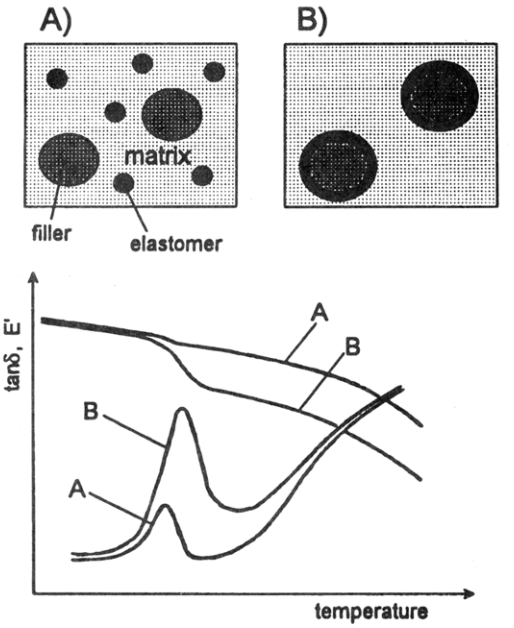

Figure 10. Influence of the morphology on the dynamic mechanical behavior in composites consisting of a glassy matrix, a rigid filler, and an elastomer according to Ishida and Jay:[35] (A) elastomer dispersed in the glassy matrix without connection to the rigid filler; (B) rigid filler covered by the elastomer.

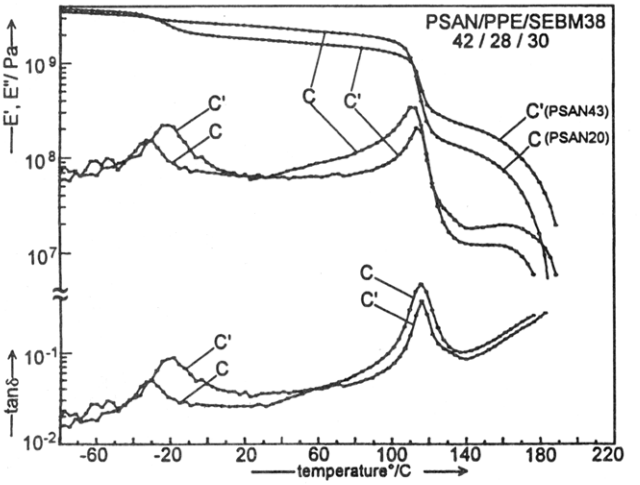

Figure 11. Dynamic mechanical behavior of blends C and C′ (see Table III) containing PSAN20 and PSAN43, respectively. Dual cantilever geometry at 1 rad s^{-1}.

Table IV[a]

	wt %			SEBM38		SEBM17	
no.	PSAN20	PPE-II	SEBM	w_{PMMA}	w_{PS}	w_{PMMA}	w_{PS}
a	0	70	30	1	0.093	1	0.171
b	14	56	30	0.449	0.114	0.429	0.205
c	28	42	30	0.289	0.149	0.273	0.255
d	42	28	30	0.213	0.204	0.200	0.340
e	56	14	30	0.169	0.340	0.158	0.507
f	70	0	30	0.140	1	0.130	1

[a] w_{PMMA} = weight fraction of PMMA on the basis of PMMA and PSAN; w_{PS} = weight fraction PS on the basis PS and PPE.

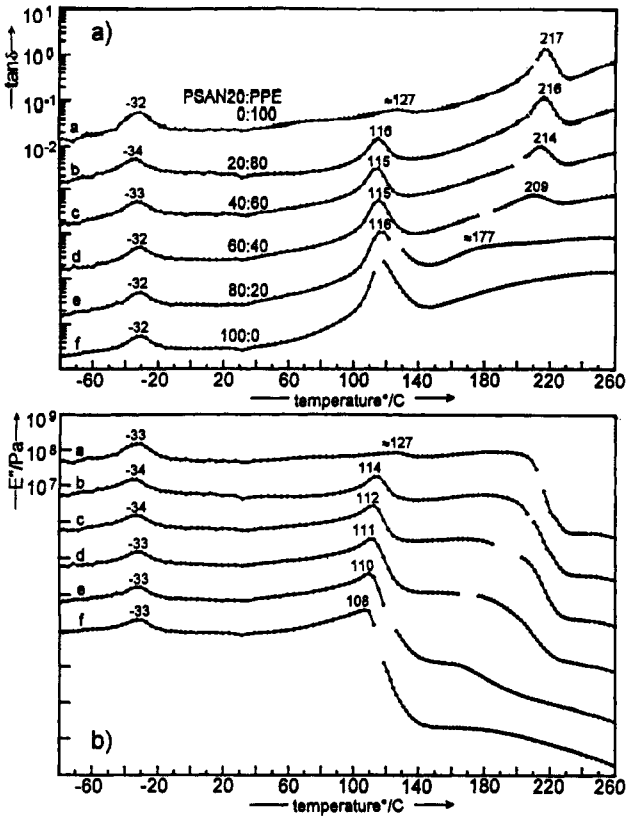

Figure 12. Dynamic mechanical analysis (tan δ and E'') of ternary blend (a–f) PSAN20:PPE; x:y)/SEBM38 (70:30) dual cantilever ($E'' > 10^7$ Pa) and shear sandwich ($3G'' = E'' < 10^7$ Pa) geometry. For detailed compositions, see Table IV. Data for different experiments are shifted vertically for one decade. The ordinate axis is valid for the upper curve.

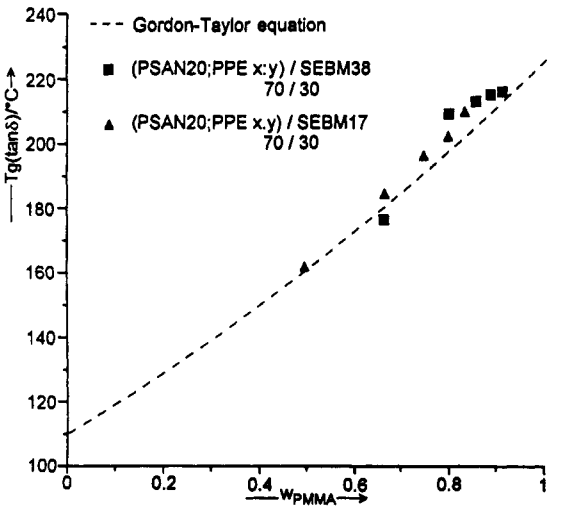

Figure 13. Glass transition of the mixed PS/PPE phase in ternary PSAN20/PPE/SEBM blends ($T_{g(PS/PPE)}$ taken as tan δ_{max}) as a function of the weight fraction of PPE w_{PPE} ($=m_{PPE}/(m_{PPE} + m_{PS})$). The dashed curve corresponds to the predictions of the Gordon Taylor equation, which describes binary PPE/PS mixtures. Key: (■) (PSAN20:PPE; x:y)/SEBM38 (70:30); (▲) (PSAN20:PPE; x:y)/SEBM17 (70:30).

The whole surface of the PPE domains is covered by ellipsoidal PEB particles, resembling a raspberry type morphology (Figures 8c,d and 9c,d). As will be shown below, this morphology is independent of the blend composition. Figure 9e summarizes the dimensions for the PEB domains taken from a more detailed TEM analysis. The morphology of the blends containing SEBM38 shows some of the characteristics observed in the pure block copolymers containing a lower amount of elastomeric center block. The transition of a layerlike

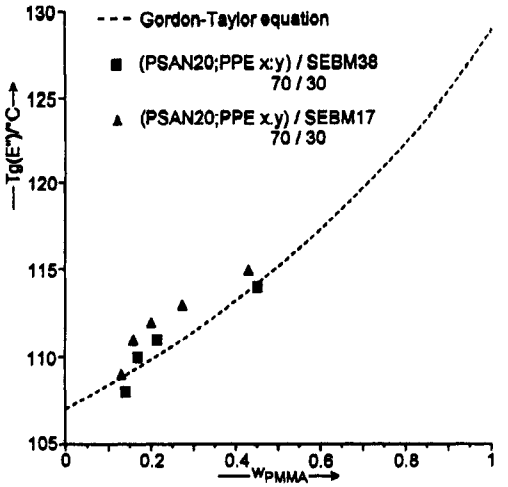

Figure 14. Glass transition (E''^{max}) of the mixed PSAN20/PMMA phase in ternary blends containing SEBM38 and SEBM17 as a function of the PMMA weight fraction w_{PMMA} ($=m_{PMMA} + m_{PSAN}$)): (■) (PSAN20:PPE; x:y)/SEBM38 (70:30); (▲) (PSAN20:PPE; x:y)/SEBM17 (70:30). The dashed curve corresponds to the Gordon Taylor equation, using the parameters ($T_{g(PSAN)}$, $T_{g(PMMA)}$, K) which describe corresponding binary blends of PSAN20 and PMMA.

PEB phase or PEB matrix to isolated, highly constrained microdomains is associated in both cases with a lowering of the elastomer glass transition. The reason for the formation of isolated PEB particles in contrast to an extended PEB layer surrounding the dispersed PPE phase (Figure 2) is the high surface energy between PEB and PS or PMMA, respectively. Direct comparison of blends with PSAN43 and PSAN20 (Figures 7 and 8) shows that the block copolymer is a more efficient emulsifier in the latter case. The dynamic mechanical properties can be compared to the behavior of composites consisting of a glassy polymer matrix, a dispersed filler, and a dispersed rubber.

According to Ishida and Jay[35] the dynamic mechanical response at the same overall composition depends on the distribution of filler and rubber particles (Figure 10). In case A (Figure 10A) filler and rubber are dispersed independently in the glassy matrix; there is a direct connection between the filler and the matrix. Case B describes the situation where the rubber completely covers the filler. At constant composition theory predicts that the modulus at the elastomer glass transition drops more strongly in case B compared to case A due to an increased mechanical damping. Figure 11 shows the direct comparison of ternary blends with PSAN20 and PSAN43 at the same overall composition for the blend containing 30 wt % SEBM38. The PSAN43 blend shows a more pronounced PEB glass transition and a considerable lower storage modulus between $T_{g(PEB)}$ and $T_{g(PSAN)}$. Above the $T_{g(PSAN)}$ the higher melt modulus of PSAN43 compared to PSAN20 dominates the response. The same results are obtained for blends containing 15 wt % SEBM38, while no difference exists below $T_{g(PSAN)}$ in binary blends without block copolymer. This corresponds to a complete coverage of the PPE filler particles by an elastomer layer.

Obviously, the raspberry morphology, where the glassy filler and the glassy matrix are directly connected (Figure 9) has the same characteristics as the situation described by Figure 10A with direct contacts of matrix (PSAN) and filler (PPE).

B. Variation of the Blend Composition at Constant Fraction of P(S-*b*-EB-*b*-MMA). Figure 3b shows the blend compositions studied in the present section. P(S-*b*-EB-*b*-MMA) (30 wt %) triblock copolymers SEBM38 and SEBM17 were used. The detailed compositions are

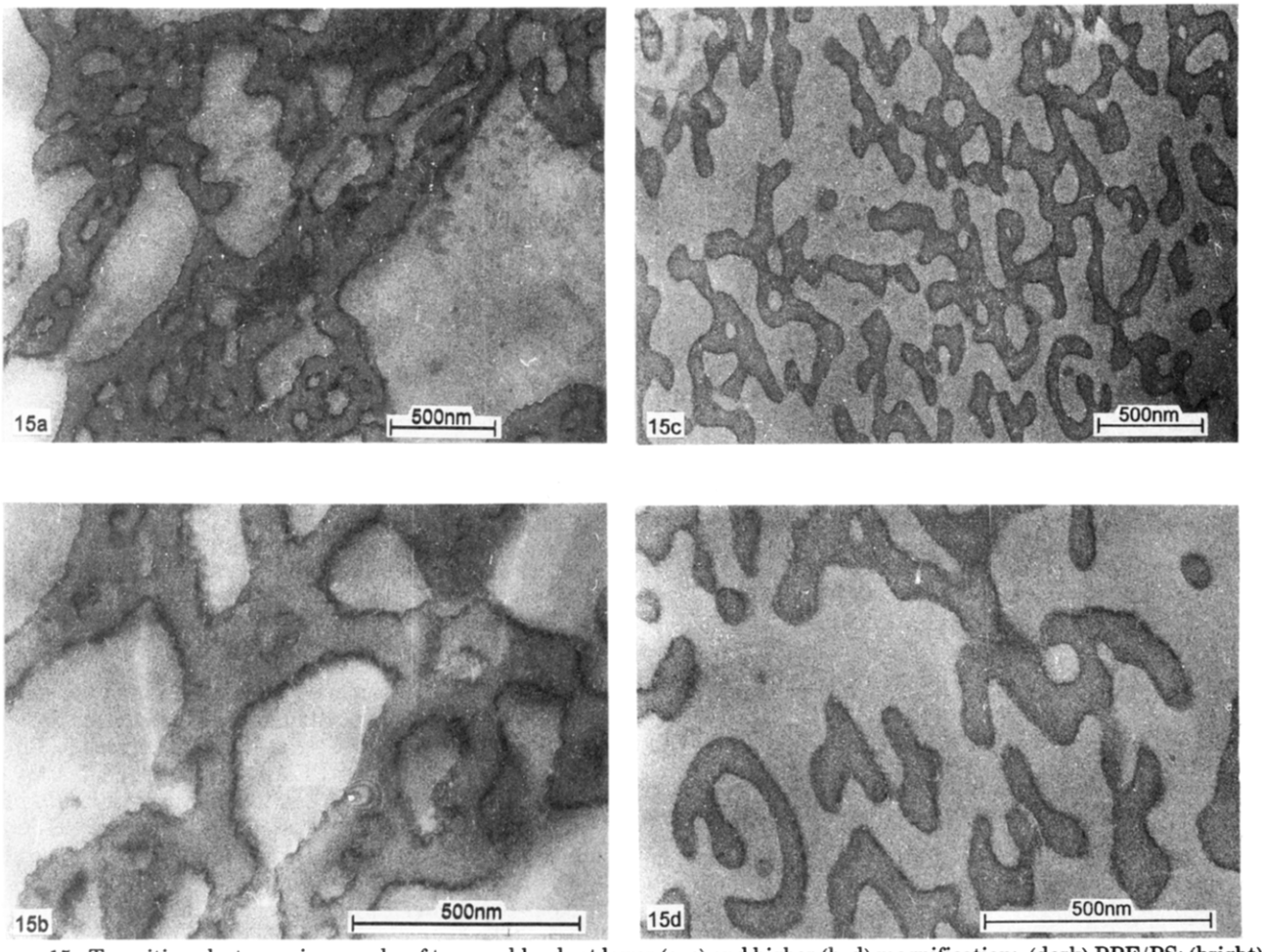

Figure 15. Transition electron micrographs of ternary blends at lower (a, c) and higher (b, d) magnification: (dark) PPE/PS; (bright) PSAN/PMMA; (a, b) PSAN20/PPE/PPE/SEBM17 (50:34:16) (=60:40:20); (c, d) PSAN20/PPE/SEBM6 (50:34:16). The EB microdomains can be recognized as regular indents along the PPE domains.

listed in Table IV. Due to the relatively large amount of block copolymer it is possible to study the PEB glass transition. The overall content is 11.4 wt % in the case of SEBM38 and 5.1 wt % in the case of SEBM17. In the latter case the measurements at low temperatures were made at 10 rad s^{-1} to reduce the noise.

Figure 12 shows the E'' and tan δ data for PSAN20/PPE/SEBM38 blends (a–f). Independent of the blend composition, the PEB glass transition is located around −33 °C. The glass transition of both the PPE/PS and the PSAN20/PMMA mixed phases show the expected behavior: $T_{g(PPE/PS)}$ is analyzed from the maximum of tan δ. The experimental data are close to the values expected for a homogeneous binary PPE/PS mixture (Figure 13). As explained in the preceding section, the slightly higher experimental values in the case of the ternary blends can be explained on the basis of the relatively low molecular weight of the PS block.[9] For SEBM17 with a PS block molecular weight around 100k, the agreement between the present experimental data and the values expected for a completely homogeneous intermixing of PS and PPE is better.

Figure 14 shows the corresponding analysis of the PSAN/PMMA glass transition. In this case the loss modulus maximum E''^{max} has been used as the measure for $T_{g(PSAN/PMMA)}$. Again the data are in reasonable agreement with the values expected for a homogeneous PSAN/PMMA mixture. The DMA of the different blend compositions *a–f* shows that for block copolymers SEBM38 and SEBM17 the same structural principles are valid. Obviously, the block copolymers are all located at the phase boundary. The PS and PMMA blocks are mixed into the PPE and PSAN20 phases, respectively, while the PEB block forms isolated microdomains, as indicated by the low T_g. Figure 15a,b shows TEM micrographs of blends containing SEBM17 and SEBM6 at two different magnifications. The staining conditions were identical to those used for Figure 8a,b. As expected from the dynamic mechanical data, the same morphological features in PSAN20/PPE/SEBM38 blends are observed. Even for the blend with SEBM6, where the PEB block has a molecular weight of only about 10k, the modulated surface can be recognized. The estimated size of the PEB microdomains is on the order of 5–10 nm. Because of the low rubber content in the blend (about 1 wt %) the PEB glass transition cannot be determined by DMA.

Figures 8a,b and 15a–d allow the comparison of the emulsifying efficiency of the different block copolymers SEBM38, SEBM17, and SEBM6 at the same overall blend composition. All blends have a bicontinuous morphology

Table V[a]

			SEBM38		SEBM17		SEBM6	
PSAN20	PPE-II	SEBM	w_{PMMA}	w_{PS}	w_{PMMA}	w_{PS}	w_{PMMA}	w_{PS}
			Composition D					
60	40	20	0.112	0.107	0.104	0.194	0.140	0.184
			Composition E					
80	20	5	0.023	0.057	0.021	0.107	0.030	0.101

[a] w_{PMMA} = weight fraction of PMMA on the basis of PMMA and PSAN; w_{PS} = weight fraction PS on the basis PS and PPE.

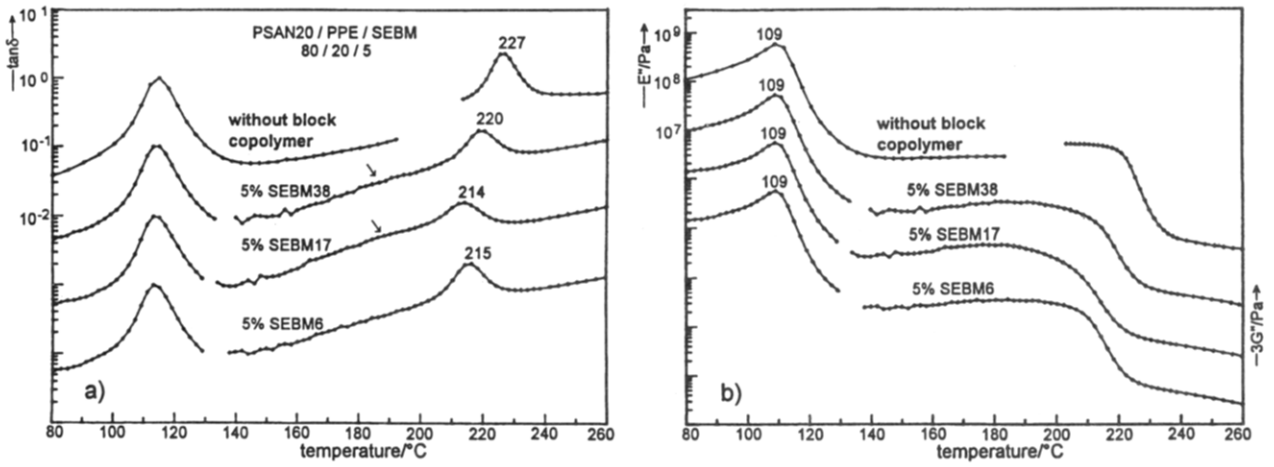

Figure 16. Dynamic mechanical analysis of blends PSAN20/PPE/SEBM (80:20:5). Combined set of dual cantilever and shear sandwich data at 1 rad s^{-1}: (a) (tan δ)/T, (b) E''/T. The data for the different blends are shifted vertically by one decade. The ordinate axis is valid for the upper curve.

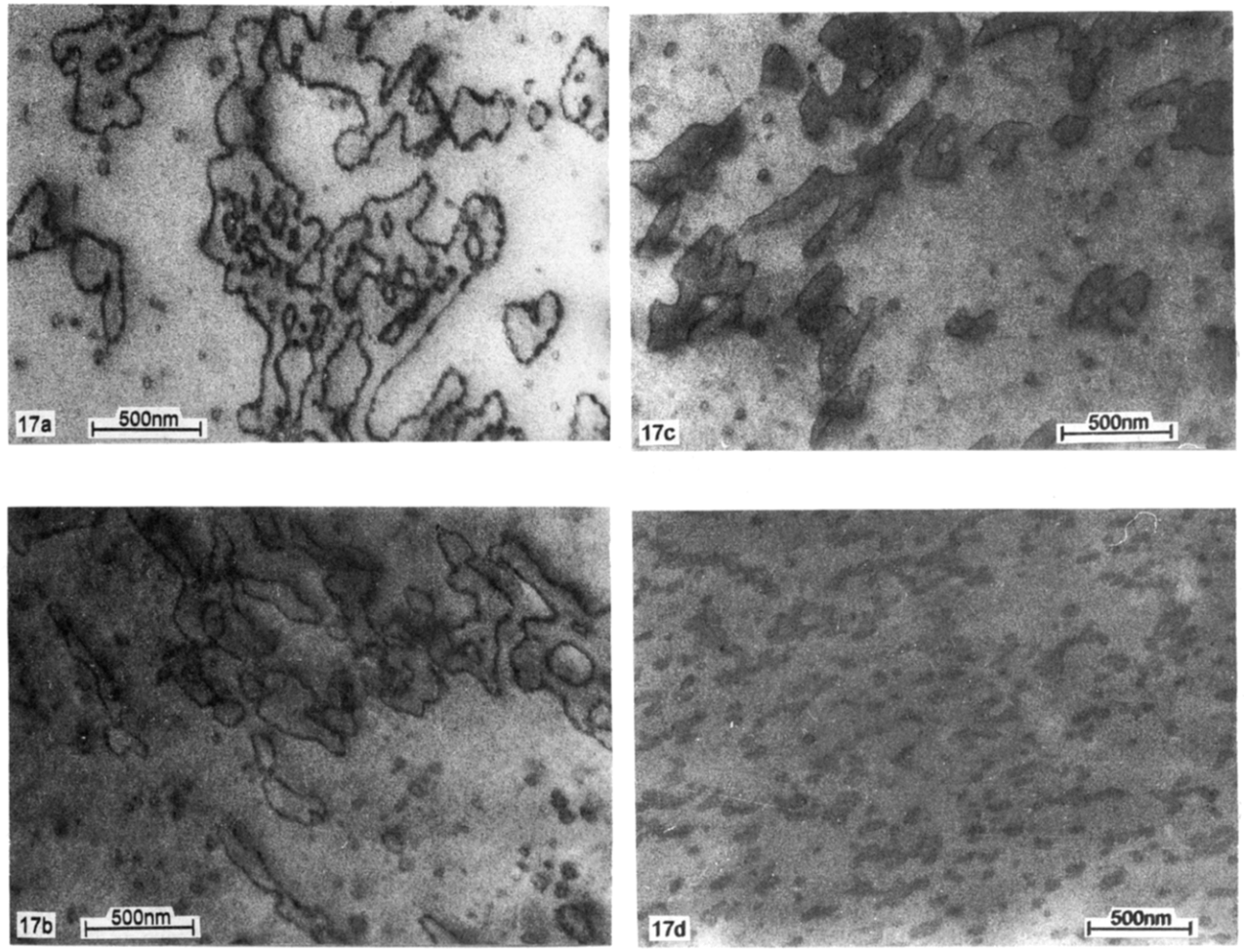

Figure 17. TEM micrographs of PSAN20/PPE blends with PSAN20 as the matrix phase and small amounts of various block copolymers (PSAN20/PPE/block copolymer) (80:20:5): (a) SEBM38; (b) SEBM17; (c) SEBM6; (d) SM78 (diblock).

with typical diameters of the PPE domains on the order of 50–100 nm. Thus the major part of the PPE is accessible to the PS blocks emerging from the PEB microdomains. This already has been deduced from the changes of the PPE glass transition. Figures 8a,b and 15a also show that the PSAN forms larger domains (500 nm to 1 μm). No homogeneous intermixing of the PSAN chains with the PMMA block is possible on this length scale. In general the structures are larger than in corresponding blends with P(S-*b*-MMA) diblock copolymers (see below). This also explains why these blends with P(S-*b*-EB-*b*-MMA) triblocks are slightly turbid. In the case of added diblock we never observed such an irregular bicontinuous distribution of the microphases. As a general trend the system tends to attain a homogeneous intermixing of PS and PPE. In the case of blends with SEBM6 the morphology is much more homogeneous. The emulsifying characteristics of SEBM6 are closer to those of a P(S-*b*-MMA) diblock.

C. Ternary Blends with Small Amounts of Block Copolymer. So far only blends with a PSAN:PPE ratio of 60:40 have been considered in the morphological studies at a large level of added block copolymers. It has been

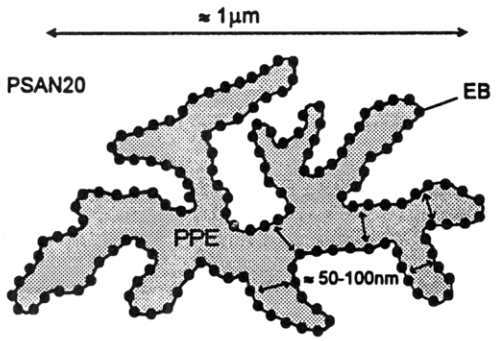

Figure 18. Schematic representation of the dimensions and the structure of a PPE domain in ternary PSAN20/PPE/SEBM blends in the case of a PSAN20 matrix.

Table VI. Glass Transitions (°C) for PS/PPE Mixed Phase in Ternary PSAN/PPE/SEBM (80:20:5) Blends (Composition E)

	SEBM 38	SEBM 17	SEBM 6
expected	218	212	212
experimental	220	214	215

shown that this composition tends to result in a bicontinuous morphology. In the following section blends with a PSAN:PPE ratio of 80:20 with a small amount (5 parts per hundred) of various block copolymers are studied to check whether the same morphological features are present in the case of a dispersed PPE phase with a considerably smaller amount of block copolymer.

Blends of composition E (see Figure 3c, Table V) were prepared using the triblock copolymers SEBM38, SEBM17, and SEBM6 and a diblock coplymer SM 97 which has approximately the same length of the PS and PMMA block as the triblock copolymers. Figure 16a,b shows the dynamic mechanical analysis (tan δ and E'') of the blends containing the triblock copolymers in comparison to the blend without block copolymer. Due to the small fraction of elastomer (<1.8 wt %) no attempt to analyze the PEB glass transition has been made. The DMA data show that $T_{g(PSAN)}$ is not influenced by the addition of the block copolymer. The expected shift of $T_{g(PSAN)}$, which would be observed if PMMA and PSAN20 segments are mixed homogeneously, is below 1 deg. However, penetration of the PS block into the PPE phase results in a detectable reduction of the PPE glass transition.

Table VI compares the experimental value of the glass transition with those expected for a completely homogeneous mixture. The data show that independent of the triblock the PS/PPE phase is rather homogeneously mixed. For SEBM38 and SEBM17 a slight broadening of the transition is observed, indicating a broader segment density gradient.[9] Parts a–c of Figure 17 show the corresponding TEM micrographs. The blend with SEBM38 (Figure 17a) nicely shows the pearl string morphology characteristic for the isolated PEB microdomains along the PSAN/PPE interface. The diameters are on the order of 15–30 nm. The same morphology is also present in the blend with SEBM17 (Figure 17b) with a smaller PEB domain. If SEBM6 is used as compatibilizer (Figure 17c), the micrograph does not allow a detection of the elastomer domains. This is not surprising because the elastomer content is only 0.3 wt % (1.8 wt % in the SEBM38 blend, 0.8 wt % in the SEBM17 blend). However, the different morphology of the blend containing SEBM6 as compared to the blend containing the diblock copolymer (Figure 17d) indicates that the PEB still forms individual microdomains along the phase boundary.

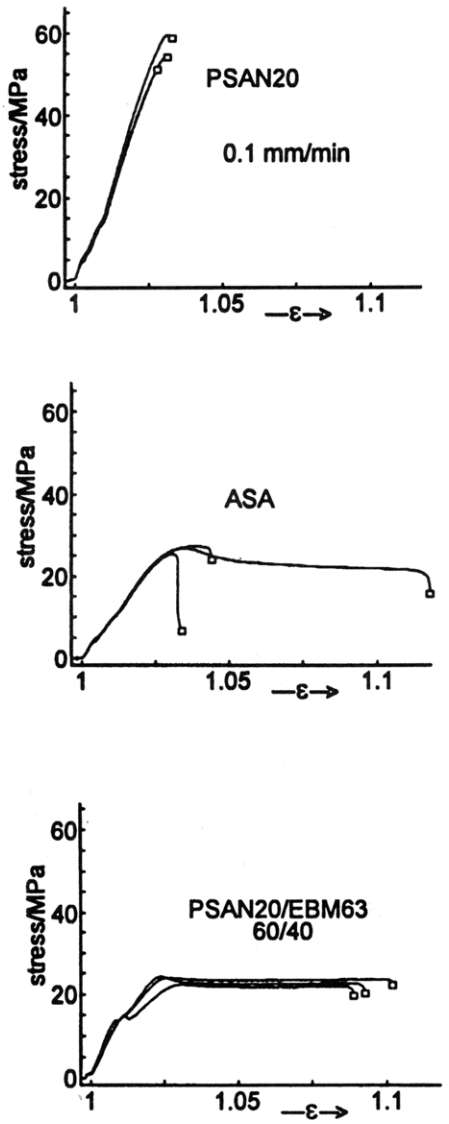

Figure 19. Stress strain behavior of pure PSAN20 (a, top), technical grade ASA (b, middle), and PSAN20 toughened by the addition of a P(EB-*b*-MMA) diblock copolymer (PSAN20^t = PSAN20 + EBM63 (70:30)) (c, bottom). The rubber content in ASA and PSAN20^t is the same.

The blend with the SM97 diblock copolymer (Figure 17d) shows very homogeneous regular particles with diameters in the range 50–150 nm.[9] In contrast the PPE particles in the blends with the SEBM triblocks have a highly irregular shape. The longest distance to the PSAN phase boundary is not more than 25–50 nm; however the overall size of a PPE particle is on the order of 1–2 μm in the case of SEBM38, about 0.5–1 μm in the case of SEBM17, and 0.3–0.6 μm in the case of SEBM6 as emulsifier. In the last case the surface is less rugged. Figure 18 gives a schematic representation of a PPE domain in a ternary PSAN20/PPE/SEBM blend in the case of a PSAN20 matrix, summarizing the characteristic dimensions as taken from the micrographs.

D. Ultimate Properties of PSAN/P(S-*b*-EB-*b*-MMA)/PPE Blends. Two types of experiments were performed to test whether the SEBM triblock copolymer has a positive effect on the ultimate tensile properties. First, simple stress–strain experiments were performed. However, due to the brittleness of untoughened PSAN20 no information about the weakness or strength of the PPE/PSAN20 interface could be obtained. To elucidate the influence of block copolymers as mechanically effective

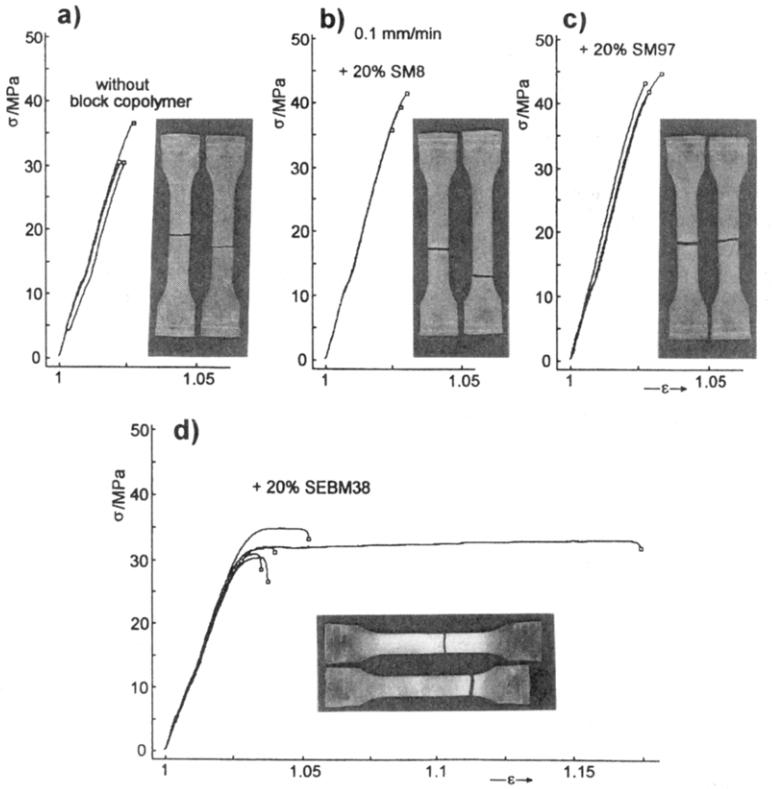

Figure 20. Stress strain behavior of PSAN20[t]/PPE blends: (a) without block copolymer (60:40); (b) with low molar mass diblock copolymer SM8 (for synthesis and characterization see ref 9) (60:40:20); (c) with high molar mass diblock copolymer SM97 (60:40:20); (d) with SEBM38 (60:40:20). Photographs show a typical specimen.

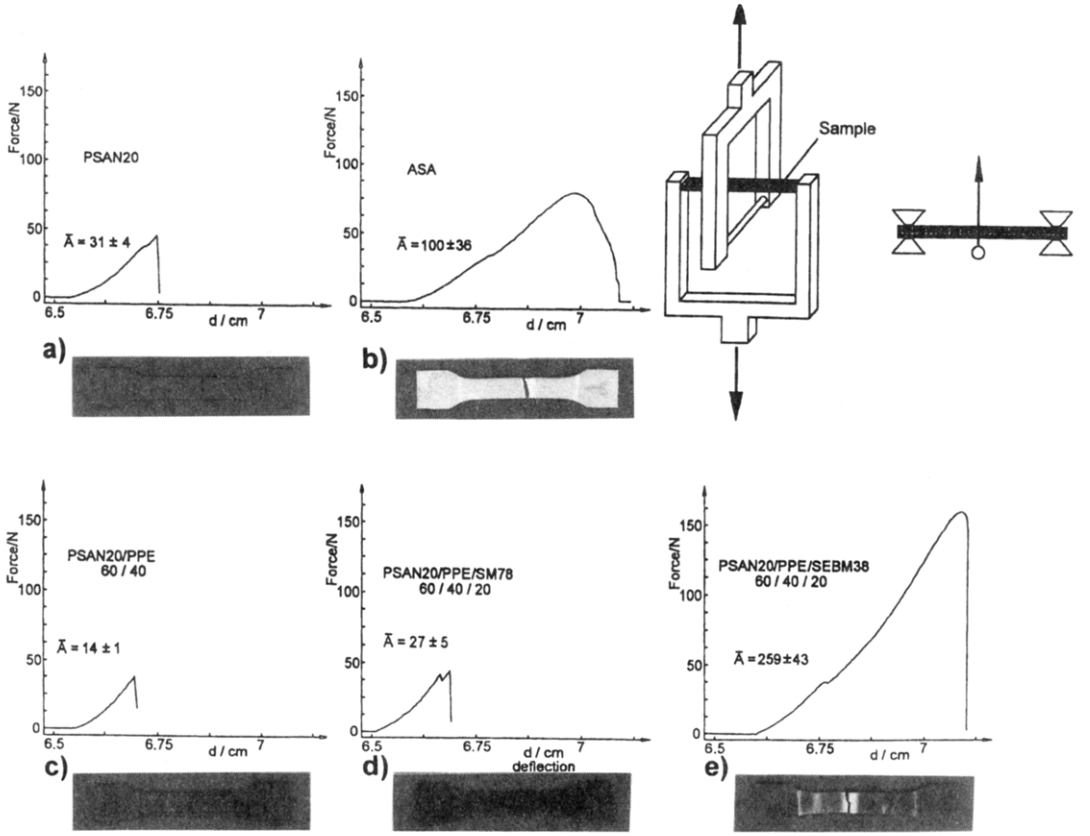

Figure 21. Ultimate properties in the bending test (crosshead speed: 1 mm/min). Photographs show a typical specimen. Areas of the force-deformation experiments and standard deviations resulted from three tests. Key: (a) PSAN20 (pure material, not toughened); (b) ASA (technical grade); (c) PSAN20/PPE (60:40); (d) PSAN20/PPE/SM97 (60:40:20); (e) PSAN20/PPE/SEBM38 (60:40:20).

interfacial agents in PSAN/PPE blends, a rubber toughened PSAN has been used. Because technical ABS or ASA grade polymers cannot be subjected to the method of blend preparation used in this study, PSAN20 was rubber toughened by the addition of 30 wt % of P(EB-*b*-PMMA) diblock copolymer (detailed characterization, see Table 1). Addition of this diblock copolymer to PSAN20 results in an efficient toughening of PSAN

(PSAN20^t = PSAN20 + EBM63 (70:30)). Under the experimental conditions of the stress–strain experiment the material is comparable to technical grade of ASA (Figure 19a,b).

In a first set of experiments this rubber toughened PSAN20^t (PSAN20 + EBM63 70:30) was used in blends with PPE and additional block copolymer. Figure 20 shows that the blends of high molecular weight PPE with toughened PSAN20^t with and without added P(S-*b*-MMA) diblock copolymers of two different molecular weights remain brittle despite the fact that the block copolymer efficiently locates at the PSAN20/PPE phase boundary.[9]

Only addition of the block copolymer with the elastomeric center block improves the ultimate properties. In comparison with blends containing only diblock copolymer extended areas of strain whitening indicate efficient craze generation (Figure 20). Characteristic specimens are also shown in Figure 20. In all other blends brittle fracture is observed.

In a second set of experiments an experimental setup has been designed for small scale laboratory testing where a deformation mode analogous to standard fracture tests has been used (Figure 21). A sample is subjected to large deformations in the bending mode. At constant sample geometry, the area under the stress deformation curve is proportional to the fracture energy.[36] In comparison to the simple stress–strain testing, this setup is less sensitive to small surface defects of the samples. Due to the limited time resolution of the data aquisition, a relatively small deformation rate was chosen. Comparison of neat PSAN20 with technical grade ASA shows that the test allows a clear distinction between brittle and tough materials. Figure 21 shows typical experimental curves of this test. The areas indicated on the figure are the average of three tests. Reproducibility turned out to be rather good. According to these results the fracture energy of the technical grade ASA which contains about 28 wt % of acrylate rubber is about 3 times as large as that of pure PSAN20. The PSAN20/PPE blend without block copolymer is even more brittle than the pure PSAN20. Upon addition of a P(S-*b*-MMA) diblock copolymer with large blocks about the same values are obtained for the PPE/PSAN blend as for the pure PSAN. Addition of SEBM38 results in a drastic increase of the fracture energy. The area is increased by a factor of 18 compared to the case of PSAN20/PPE blend. The area under the force deformation curve is even 2.5 times as large as that for the technical grade ASA, though the overall rubber content in the PSAN20/PPE/SEBM38 blend is only 6.8 wt % while the ASA has a much higher rubber content. The specimen with SEBM38 as compatibilizing agent also shows craze formation in these blends where PSAN20 (not PSAN20^t!) has been used.

Conclusions and Outlook

It has been shown in the preceding sections that the elastomeric center block of P(S-*b*-EB-*b*-MMA) triblock copolymers has a dominating influence on the morphology and the mechanical response of PSAN20/PPE blends compatibilized by these triblock copolymers. As in blends with P(S-*b*-MMA) diblock copolymers the triblock copolymer locates at the interface of the blend. Due to the thermodynamic driving force the PS and the PMMA blocks efficiently intermix with the blend components PPE and PSAN20, generating a wet brush situation (see Figure 1). Due to the strong incompatibility of the elastomeric center block to all other components the PPE/PSAN20 phase boundary is covered with small ellipsoidal rubber islands and not with a surrounding rubbery layer. Due to this morphology the block copolymer not only improves phase adhesion, but the small PEB microdomains located at the PPE/PSAN phase boundary obviously play a dominating role in changing the fracture behavior.

It is reasonable to assume that the small PEB microdomains with a perfect phase adhesion to both major blend components act as stress centers and help to initiate stable crazes. These would absorb a lot of energy before fracture. The extended stress whitened areas observed in the blends with added SEBM38 support this interpretation. Though the triblocks are less effective emulsifiers in terms of the size of the dispersed particles, this has no negative effect on the mechanical response. It even may be an advantage, because the resulting rubber covered PPE domains have characteristic dimensions on the order of 1 μm.

The data show that a new design of block copolymer compatibilizers successfully combines high modulus (low rubber content) with toughness. In addition low temperature toughness should be improved due to the lowering of the elastomer glass transition, which is another interesting aspect of these spatially confined elastomer chains.

P(A-*b*-E-*b*-B) triblock copolymers with an incompatible elastomeric (E) center block may be successful for compatibilizing other glassy polymer blends. On the basis of the present results studies are in progress to clarify the role of block copolymer composition and molecular weight on the blend properties.

Acknowledgment. This work has been supported by the Ministry of Science and Technology (Grant 03M4041) and BASF AG within the project "Neue Polymerlegierungen durch Reactive Blending". Further support from the Deutsche Forschungsgemeinschaft (SFB262, Project S14) is gratefully acknowledged. The authors are grateful to Dr. K. Mühlbach and Dr. A. Gottschalk (BASF AG) for intense discussions and providing the ASA and PSAN copolymers. The TEM micrographs were made at the Institute for Physical Chemistry, Mainz, with the technical assistance of R. Würfel in the laboratory of Dr. I. G. Voigt-Martin.

References and Notes

(1) (a) Utracki, L. A. *Polymer Alloys and Blends*; Hansa Publishers: Munich, 1990. (b) Paul, D. R. *Polymer Blends*; Academic Press: New York, 1978; Chapter 12.
(2) Leibler, L. *Makromol. Chem., Makromol. Symp.* **1988**, *16*, 1.
(3) (a) Noolandi, J.; Hong, K. M. *Macromolecules* **1982**, *15*, 482. (b) Noolandi, J.; Hong, K. M. *Macromolecules* **1984**, *17*, 1531.
(4) Bucknall, D. G.; Higgins, J. S.; Rostami, S. *Polymer* **1992**, *33*, 4419.
(5) Brown, H. R.; Char, K.; Deline, V. R.; Green, P. F. *Macromolecules* **1993**, *26*, 4155. Char, K.; Brown, H. R.; Deline, V. R. *Macromolecules* **1993**, *26*, 4164. Brown, H. R. *Macromolecules* **1991**, *24*, 2752.
(6) Creton, C.; Kramer, E. J.; Hadziiouannou, G. *Macromolecules* **1991**, *24*, 1846.
(7) Braun, H.; Cantow, H. J. *Makromol. Chem., Theory Simul.* Submitted for publication.
(8) Auschra, C.; Stadler, R.; Voigt-Martin, I. *Polymer* **1993**, *34*, 2081.
(9) Auschra, C.; Stadler, R.; Voigt-Martin, I. *Polymer* **1993**, *34*, 2093.
(10) Kambour, R. P.; Bendler, J. T.; Boop, R. D. *Macromolecules* **1983**, *16*, 753.
(11) Estimated from the segment interaction parameters $\chi_{S,MMA}$ and χ_{AN}, given by Kammer et al.[12] according to $\chi_{PSAN20} = \beta\chi_{S,MMA} + (1-\beta)\chi_{AN,MMA} - \beta(1-\beta)\chi_{S,AN}$.[13]
(12) Kammer, H. W.; Kressler, J. *Makromol. Chem.* **1988**, *18*, 63.
(13) ten Brinke, G.; Karasz, F. E.; MacKnight, W. J. *Macromolecules* **1983**, *16*, 1827.
(14) Auschra, C. Doctoral Dissertation, Johannes Gutenberg-Universität Mainz, 1992.

(15) Heikens, D.; Hoen, N.; Barentsen, W.; Piet, P.; Ladan, H. *J. Polym. Sci. Symp.* **1978**, *62*, 309.
(16) Fayt, R.; Jerome, R.; Teyssie, Ph, *J. Polym. Sci., Polym. Phys. Ed.* **1982**, *20*, 2209.
(17) Auschra, C.; Stadler, R. *Polym. Bull.* **1993**, *30*, 257.
(18) Auschra, C.; Stadler, R. *Macromolecules* **1993**, *26*, 2171.
(19) Riess, G. In *Thermoplastic Elastomers. A Comprehensive Review*; Ledge, N. R., Holden, G., Schroeder, H. E., Eds.; Hanser Publishers: Munich, New York, 1987; Chapter 12.2, pp 325 ff.
(20) Riess, G.; Schlienger, M.; Marti, S. *J. Macromol. Sci.* **1980**, *B17* (2), 355.
(21) Riess, G. *Angew, Makromol. Chem.* **1977**, *60/61*, 21.
(22) Mogi, Y.; Kotsuji, H.; Kaneko, Y.; Mori, K.; Matsushita, Y.; Noda, I. *Macromolecules* **1992**, *25*, 5408. Mogi, Y.; Mori, K.; Matsushita, Y.; Noda, I. *Macromolecules* **1992**, *25*, 5412.
(23) Arai, K.; Kotaka, T.; Kitano, Y.; Yoshimura, K. *Macromolecules* **1980**, *13*, 1670.
(24) Matsushita, Y.; Yamada, K.; Hattori, T.; Fujimoto, T.; Sawada, Y.; Nagasawa, M.; Matsui, C. *Macromolecules* **1983**, *16*, 10.
(25) Mango, L. A.; Lenz, R. W. *Makromol. Chem.* **1973**, *163*, 13.
(26) Auschra, C.; Stadler, R. *Polym. Bull.* **1993**, *30*, 305.
(27) The authors are indebted to Mr. F. Herzog, Institut für Makromolekulare Chemie, Freiburg, for performing the membrane osmometrical measurements.
(28) Percec, V.; Shaffer, T. D. *J. Polym. Sci., Polym. Lett. Ed.* **1986**, *24*, 439.
(29) Trent, J. S.; Scheinbein, J. I.; Couchman, P. R. *Macromolecules* **1983**, *16*, 589.
(30) de Araujo, M. A.; Stadler, R.; Cantow, H-J. *Polymer* **1988**, *29*, 2235.
(31) Prest, W. M.; Porter, R. S. *J. Polym. Sci., Polym. Phys. Ed.* **1972**, *10*, 1639.
(32) Auschra, C.; Beckmann, J.; Voigt-Martin, I.; Stadler, R.; Leibler, L. Manuscript in preparation.
(33) Bates, F. S.; Berney, C. V.; Cohen, R. E. *Macromolecules* **1983**, *16*, 1101. Bates, F. S.; Cohen, R. E.; Argon, A. S. *Macromolecules* **1983**, *16*, 1108.
(34) An enhanced contrast at the phase boundary is also observed in other staining techniques, i.e. in staining of the amorphous/crystal interface in semicrystalline polyethylene. It could be due to an enrichment of the staining agent at the phase boundary.
(35) Ishida, H.; Jay, J. *Makromol. Chem., Macromol. Symp.* **1988**, *22*, 191.
(36) Kausch, H. H. *Polymer Fracture*, 2nd ed.; Springer: Berlin, 1987.